Acta Acustica united with Acustica
Vol. 103 (2017) 1025 – 1036

DOI 10.3813/AAA.919132

On the Optimisation of Multi-Degree-of-Freedom Acoustic Impedances of Low-Frequency Electroacoustic Absorbers for Room Modal Equalisation

Etienne Rivet, Sami Karkar, Hervé Lissek
Signal Processing Laboratory LTS2, École polytechnique fédérale de Lausanne, 1015 Lausanne, Switzerland.
rivet.etienne@epfl.ch

Summary
Low-frequency electroacoustic absorbers have recently been developed as a solution for the modal equalisation. Firstly investigated in waveguides, the technique consists in matching the acoustic impedance at a closed-box loudspeaker diaphragm to the characteristic acoustic impedance of air. Extending the results in a duct to rooms brings up several challenges. Some parameters, such as the position and orientation of absorbers, the total area, as well as the acoustic impedance achieved at the diaphragms may influence the performance, especially in terms of modal decay time reduction. In this paper, the optimal values of a purely resistive acoustic impedance at an absorber diaphragm, whose area varies, are first investigated under normal incidence and grazing incidence in a finite-length waveguide. The optimal acoustic resistance values are then investigated for a given position, orientation, and total area of absorbers in rooms of different size. From these results, the target acoustic impedances with multiple degrees of freedom are defined with a view to assign to the absorber diaphragms. These impedances are then optimised from a global criterion, so that these impedances approach at best the different optimal resistance values found to minimise the modal decay times. Finally, an experimental evaluation of the performance of the electroacoustic absorber in a waveguide is provided.

PACS no. 43.20.Ks, 43.38.Dv, 43.50.Ki, 43.55.Br, 43.58.Bh

1. Introduction

Room modes cause uneven distributions in space and frequency of the sound field and alter the temporal acoustic response, resulting in long decay times [1]. This effect is particularly significant in the low-frequency range, where the modal density is low, and prevents suitable reproduction and perception of the musical content. Different strategies have been investigated to address this problem. Conventional passive absorbers are mainly used to reduce high-frequency reflections, but they are too bulky and not efficient enough for the low frequencies [2]. Optimal room ratios [3, 4, 5] and optimal placements of one or multiple sound sources [6, 7, 8, 9] were also investigated to reduce the audible effects caused by the resonances. Active corrections have received much attention in the last decades for the low-frequency room equalisation. Equalising the frequency response at a single listening position might cause a degradation of the frequency responses at other locations. With multiple-input/-output techniques, the equalisation zone can be significantly extended [10, 11, 12]. Several local and global criteria were proposed, such as the minimisation of the potential energy [13], the minimisation of the sound power [14], as well as the minimisation of the modal decay times [15]. For rectangular rooms and symmetrical loudspeaker arrangement, the equalisation can also be achieved by simulating a progressive plane wave, thanks to secondary loudspeakers located at the opposite wall of the sound sources, with error sensors [16, 17], or only with appropriate delay and gain [18]. Nevertheless, these control methods may be costly and time consuming, and complicated to implement in rooms of irregular shape, or they might require a calibration as soon as the furniture is moved.

Another approach is the active absorption through the control of acoustic impedances. The concept of electroacoustic absorber represents an alternative solution for the modal equalisation. First developed in waveguides, the technique consists in matching the specific acoustic impedance at a loudspeaker diaphragm to the characteris-

Received 8 June 2017,
accepted 9 October 2017.

tic specific acoustic impedance of air with sensor [19], or without sensor [20]. An efficient sound absorption may be achieved over a broad frequency range, resulting in a significant damping of the first modes. Since it is obviously not realistic to cover all the walls of a room, these electroacoustic absorbers should have a physical effective surface area much smaller than the total area of the room. The optimisation of the impedance locations on the walls of an acoustic cavity was investigated in [21], to minimise the sound level generated by a velocity source. Analysing the distribution of the sound field in rooms with a given geometry makes it already possible to know where to place the absorbers for maximal performance (preferably in corners for rectangular rooms for example). Depending on the location and area of the absorber relative to the total area of the domain, the target specific acoustic impedance may differ from the characteristic specific acoustic impedance of air. The optimal acoustic impedance of absorbers under grazing incidence in flow ducts was investigated from a hybrid passive/active impedance control based on the pressure release behind a resistive layer [22, 23]. The target acoustic impedance should be determined from a representative criterion that maximises the performance of the electroacoustic absorber for the modal equalisation at any location. Such a quantity could be derived so as to minimise the dynamics of the sound pressure level at different locations as in [11]. However, with a reasonable number of frequency responses that are dependent on the locations of the source and listener, it will only give an approximate value of the dynamics of the sound pressure level. Since the modal decay times are critical for the perception of low-frequency problems [24], this quantity may also be used as a criterion as in [15]. The main advantages are that the modal decay time is related to the corresponding eigenfrequency, thus the damping coefficient of the mode. Therefore, it is independent of the locations of the source and listener in the room, and it is easily derived from analytical solutions or simulations. The modal decay times can be approximated analytically in rectangular rooms [25] or in rooms of irregular shape [26, 27] with different sound absorption coefficients on walls. As a result, the minimisation of the modal decay times is quite representative of the performance for the modal equalisation in rooms. This global criterion will be used in the following, in order to find the target acoustic impedances that will be assigned to the electroacoustic absorber diaphragms.

The paper is organised as follows: Section 2 investigates the optimal values of a purely resistive acoustic impedance at an absorber located at the end of a duct of finite length (normal incidence), with varying area. Then, the absorber is located along the wall of the duct near one of both terminations (grazing incidence). Section 3 investigates the optimal acoustic resistance values in rooms of different size, where the area and orientation of absorbers are fixed. In Section 4, multi-degree-of-freedom (MDOF) target acoustic impedances are defined and optimised, so that these impedances approach at best the different optimal acoustic resistance values found to minimise the modal decay times. Finally, in Section 5, an experimental evaluation of the performance of the electroacoustic absorber in a waveguide is provided, by applying the hybrid sensor-/shunt-based impedance control developed in [19].

2. Target acoustic impedance in duct

In this section, we study the effects of the area and orientation of an absorber on the value of the target acoustic impedance, with a view to minimise the modal decay time of the first longitudinal modes of a closed-closed duct. In the following, the air is considered as a lossless medium of propagation. We denote the characteristic specific acoustic impedance of air by $Z_c = \rho c$, where ρ is the density of air, which is equal to $1.20\,\mathrm{kg{\cdot}m^{-3}}$ at 294 K, and c is the sound speed in air, which is equal to $343.86\,\mathrm{m{\cdot}s^{-1}}$ at 1 atm and 59 % of relative humidity.

2.1. Uniform boundary condition under normal incidence

In the general case, where a sound plane wave is directed toward an absorber under normal incidence, the reflection coefficient is expressed as

$$r(\omega) = \frac{Z_{s_{\mathrm{abs}}} - Z_c}{Z_{s_{\mathrm{abs}}} + Z_c}, \tag{1}$$

where $\omega = 2\pi f$ is the angular frequency, f is the frequency, and $Z_{s_{\mathrm{abs}}}$ is the specific acoustic impedance at the absorber diaphragm, which is equal to the sound pressure over the velocity. The corresponding sound absorption coefficient is defined as

$$\alpha(\omega) = 1 - \left| r(\omega) \right|^2. \tag{2}$$

Thus, perfect sound absorption is achieved ($\alpha = 1$) when the specific acoustic impedance $Z_{s_{\mathrm{abs}}}$ at the absorber diaphragm is equal to the characteristic specific acoustic impedance of air Z_c.

Here, we consider a duct of cross-section area S_{duct} and length L with a perfectly rigid termination at one end and an absorber at the other end. The area S_{abs} of the absorber is assumed equal to the cross-section area of the duct. We denote the normalised acoustic impedance at the absorber diaphragm by $\zeta = Z_{s_{\mathrm{abs}}}/Z_c = \theta + j\chi$ where θ and χ are the normalised acoustic resistance and normalised acoustic reactance respectively. The normalised input acoustic impedance computed at the rigid end is expressed as

$$\zeta_{in}(\omega) = \frac{\zeta + \mathrm{j}\tan\left(kL\right)}{1 + \mathrm{j}\zeta\tan\left(kL\right)} = \mathrm{j}\tan\left(kL + \eta\right), \tag{3}$$

where k is the wave number and $\eta = \arctan(-j\zeta)$ [1]. The complex eigenfrequencies f_n correspond to the critical values for which the input impedance tends towards zero, namely:

$$f_n = \left(2n-1\right)\frac{c}{4L} - \eta\frac{c}{2\pi L} \tag{4}$$

for $n \in \mathbb{N}^*$.

The modal decay time $MT60_n$ of the n^{th} eigenmode, which is defined as the time needed for a sound pressure level decrease of 60 dB during the free response of the individual mode, is related to the corresponding damping coefficient δ_n [1]. It is expressed as

$$MT60_n = \frac{3\ln(10)}{\delta_n}, \tag{5}$$

where $\delta_n = 2\pi\,\mathrm{Im}(f_n)$. The modal decay time of a given mode is displayed in Figure 1, for a duct of length $L = 1.70$ m depending on the normalised acoustic resistance and normalised acoustic reactance at the absorber diaphragm. Note that the lower the acoustic reactance at the absorber diaphragm, the shorter the modal decay time. In the case where the normalised acoustic impedance ζ is equal to 1, the modal decay time tends towards zero: there is no more mode. With the aim of performing the best modal equalisation by minimising the modal decay times, the normalised acoustic impedance at the diaphragm will be assumed purely resistive in the following.

2.2. Non-uniform boundary condition under normal incidence

If the absorber area S_{abs} is smaller than the cross-section area of the duct S_{duct} and the remaining surface is considered as a hard wall, the boundary condition at this end is non uniform. Near this termination, the field is locally not uniform. When $S_{\mathrm{abs}} \lesssim S_{duct}$, the hypothesis of an almost uniform sound pressure seems reasonable. The particle velocity is equal to that of the absorber on the diaphragm, and equal to zero on the surrounding wall area. By conservation of the volume flow, this termination has an approximate effective normalised acoustic impedance $\zeta_{eff} = (S_{duct}/S_{\mathrm{abs}})\zeta$, which differs from the previous case study by a factor corresponding to the ratio of the absorber area to the duct cross-section area.

If the absorber area is substantially smaller than the duct cross-section area, the approximation does not hold any longer. An analytical approach is required to decompose the sound field on the transverse modes, as proposed in [28, 29]. This semi-analytical approach requires numerical computations to approximate some integrals. It leads to a complex nonlinear problem of size $n > 1$, caused by the contributions of numerous transverse modes, to solve the sharp boundary between the absorber diaphragm and surrounding hard wall. The longitudinal eigenmodes and corresponding eigenfrequencies of the resonator, which are dependent on the absorber area S_{abs}, can also be determined with a practical approach, namely using a finite element method, which would be more easily generalised to different geometries.

For the case where the absorber area is different from the duct cross-section area ($S_{\mathrm{abs}} \neq S_{duct}$), the results are obtained with the help of a commercial finite element method software. The duct has a square cross-section, of width $a = 30$ cm, and length $L = 1.70$ m. The absorber is modelled by a disk centred on the duct termination, whose area S_{abs} varies from 3.14 cm^2 to 314 cm^2 (that is a radius varying from 1 cm to 10 cm). To identify the optimal acoustic resistance for every configuration, the normalised acoustic impedance at the absorber diaphragm is assumed purely resistive and constant ($\zeta = \theta$). This normalised acoustic resistance θ on the disk varies from 0.1 to 10. Every model is meshed with quadratic elements of minimal size of 0.05 cm and maximal size of 5 cm. For each configuration, the eigenmodes are computed, then their corresponding values of MT60 are computed (see Equation 5).

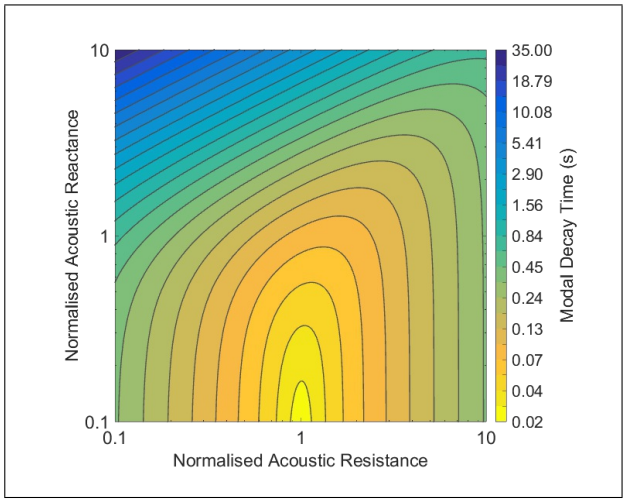

Figure 1. (Colour online) Normalised acoustic resistance – normalised acoustic reactance map of the modal decay time of a given mode in the 1D ideal case of length $L = 1.7$ m.

The results for the first three modes are presented in Figure 2. The modal decay times MT_{60} are displayed as a function of the normalised acoustic resistance θ and absorber area S_{abs}. These modal decay times are longer for non-uniform boundary conditions relative to the ideal case, where the absorber diaphragm covers the whole termination. For absorbers of sufficient area, there exists an optimal acoustic impedance value for each mode for which the modal decay time is shortened as much as possible. For example, if the absorber covers about 35 % of the duct cross-section area (that is $S_{\mathrm{abs}} = 314$ cm^2), the target normalised acoustic impedance should be set to about 0.39. Note that this impedance value decreases with the area S_{abs}. For the first mode, an absorber of area $S_{\mathrm{abs}} = 150$ cm^2, whose normalised acoustic resistance θ is equal to 1, has the same performance on this modal decay time as an absorber of $S_{\mathrm{abs}} = 50$ cm^2 with $\theta = 0.33$, or even an absorber of $S_{\mathrm{abs}} = 25$ cm^2 with $\theta = 0.17$.

Thus, if we are able to design absorbers with a low acoustic resistance value at the diaphragms for a given set of eigenfrequencies, the absorber area can be low relative to the total area of the room walls. The total number of absorbers will essentially depend on how the design, location, and orientation of these absorbers in the room can interact with the modes in the transverse directions (grazing incidence) and if they can provide an efficient damping for these modes as well, so as to minimise the modal decay times.

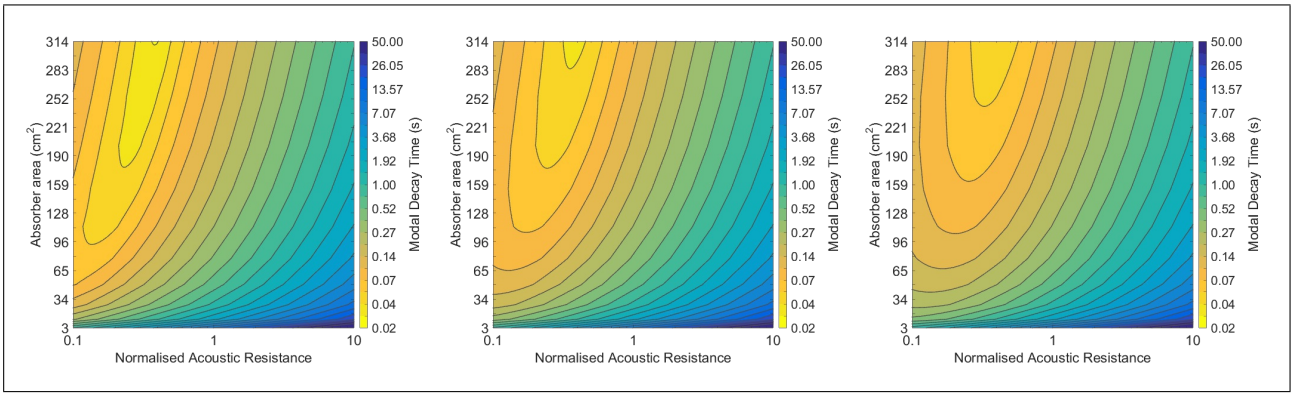

Figure 2. Normalised acoustic resistance – absorber area maps of the decay times of the (a) mode 1, (b) mode 2, and (c) mode 3 computed for an absorber under normal incidence in a duct.

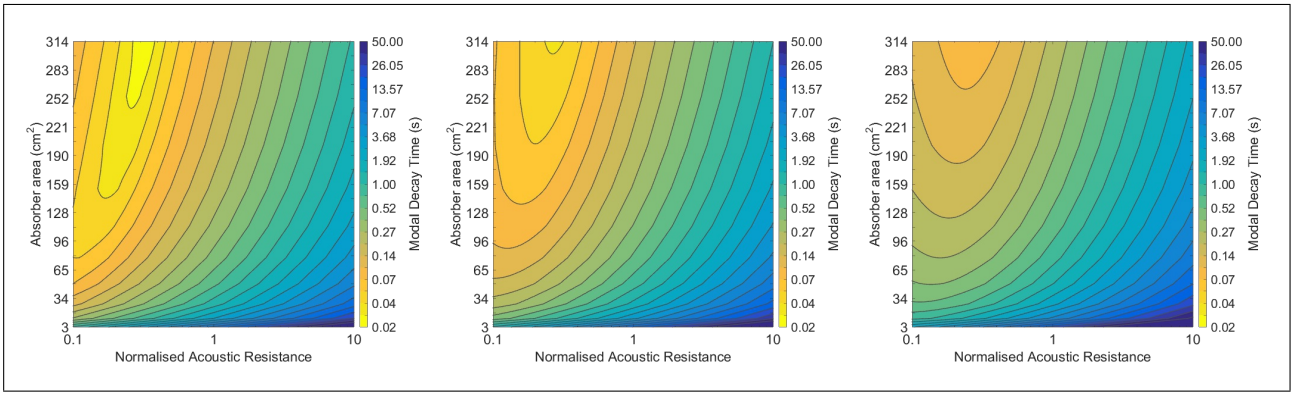

Figure 3. (Colour online) Normalised acoustic resistance – absorber area maps of the decay times of the (a) mode 1, (b) mode 2, and (c) mode 3 computed for an absorber under grazing incidence in a duct.

2.3. Non-uniform condition under grazing incidence

Under grazing incidence (that is $\theta \simeq 90°$), the sound absorption coefficient should be close to zero according to Equations (1), (2). An analytic expression for the optimal acoustic impedance of an absorptive surface covering one of the walls of an infinitely long rectangular duct was found in [30]. The analytical study gives an optimal impedance that only depends on the frequency and width of the duct. On the other hand, a duct of finite length inevitably involves reflections at both ends, resulting in other optimal values. Starting from the previous model, we study the case, where the absorber is located along the wall and whose center is at 15 cm from the duct end, so as to stay close to high sound pressure levels for the first modes. Both ends have perfectly rigid terminations; meshing and parameters are the same as in the model presented in Section 2.2.

The results for the first three modes are presented in Figure 3. The modal decay times MT_{60} are also displayed depending on the normalised acoustic resistance θ and absorber area S_{abs}. Unexpectedly, the first three modal decay times are actually shortened quite well. Its damping effect is slightly better for the first mode than under normal incidence. It is comparable for the second mode with slightly lower normalised acoustic resistances. But it is lower for the third mode. To understand these results, the sound pressure isosurfaces are displayed in Figure 4 for the first mode, in the case where $\theta = 0.25$ and $S_{\text{abs}} = 314\,\text{cm}^2$. Note how the wave fronts are locally deformed by the presence of the absorber and bend toward the absorber surface. The particle velocity is thus locally almost normal to the absorber diaphragm, instead of the expected grazing incidence. Note that this effect was previously reported in experimental results with a lined duct with grazing flow at mid frequencies [23].

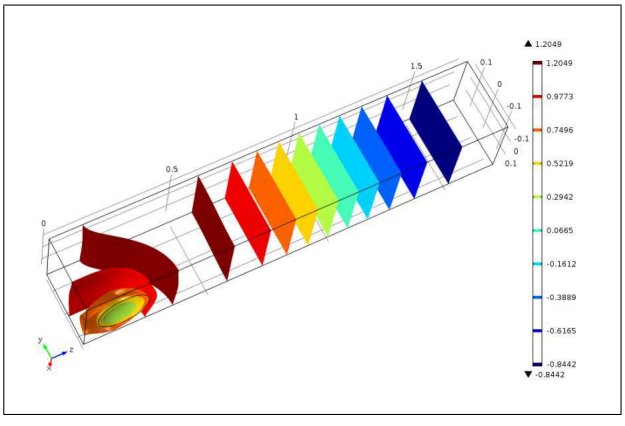

Figure 4. (Colour online) Sound pressure isosurfaces for the mode 1 in the duct with the absorber under grazing incidence (rear view), whose normalised acoustic resitance is $\theta = 0.25$ and area is $S_{\text{abs}} = 314\,\text{cm}^2$.

These results suggest that the absorber orientation has a small influence on the absorption of a mode with a given spatial structure, as long as the absorber remains sufficiently close to a maximum of sound pressure level for this mode.

3. Target acoustic impedances in rooms

From the results of Section 2, the performance of the absorber for the modal equalisation, through the minimisation of the modal decay times, depends more strongly on the area than on the orientation of the absorber in relation to the mode shape. For a given absorber area and a fixed orientation, there exists an optimal acoustic resistance that minimises the decay time of each mode. In this section, the optimal acoustic resistance values are investigated, so that the first modal decay times are shortened as much as possible, and the process is repeated for rooms of different size. For this case study, the total area of the absorbers in the rooms as well as their orientation are arbitrarily fixed.

The area of the absorber is chosen equal to 151 cm^2. To get a significant absorption area in the rooms, 16 absorbers are used for every configuration resulting in a total area S_{abs} equal to 2416 cm^2. Moreover, the results in Section 2 have shown that the absorber seems to be more efficient, when it is under normal incidence rather than under grazing incidence, except for the first axial mode in duct. As the vertical dimension generally contributes less to the first modes in usual rooms, the orientation of the absorber diaphragms normal to the axial modes along the horizontal axes is preferred. Three rooms denoted R1, R2, and R3, whose dimensions are summarised in Table I, are studied. Four boxes, each constituted of four absorbers located on two adjacent sides, are placed in the four bottom corners of the three studied rooms, as illustrated for the room R1 in Figure 5 (the absorbers are in shaded areas). The dimensions of every box is 0.3 m × 0.3 m × 0.62 m, corresponding to a global volume of around 40 dm^3.

For this case study, we intend to simulate the behaviour of actual listening rooms that have a substantial acoustic treatment at mid and high frequencies. Even though the wall acoustic reactance may shift the eigenfrequencies [1, 26], here we are only interested in the damping coefficients of the modes to estimate the modal decay times (see Equation 5). To this end, a normalised acoustic impedance $\zeta_{wall}(\omega)$ is imposed on all the walls, and we assume this impedance as purely resistive to get a corresponding sound absorption coefficient as proposed in [25, 27], and thus a given corresponding damping coefficient for the estimation of modal decay times. The acoustic resistance is also frequency dependent and is interpolated from three values equal to 78 at 10 Hz, 38 at 100 Hz, and 18 at 200 Hz, corresponding to sound absorption coefficients (under normal incidence) $\alpha = 0.05$, $\alpha = 0.10$, and $\alpha = 0.20$ respectively, according to Equation (2). The normalised acoustic impedance of the box surfaces (except the absorber diaphragms) is arbitrarily equal to 18. The purely resistive normalised acoustic impedance θ at the absorber diaphragms varied from 0.04 to 1, and the meshing and computation conditions are the same as in the previous case studie in Sections 2.2 and 2.3.

Table I. Dimensions of the rooms.

Parameter	Unit	Room R1	Room R2	Room R3
Length	m	5.33	7.02	7.87
Width	m	3.76	5.10	6.36
Height	m	2.13	2.70	3.48
Floor area	m^2	20.04	35.80	50.05
Surface area	m^2	78.80	137.05	199.15
Volume	m^3	42.69	96.66	174.18

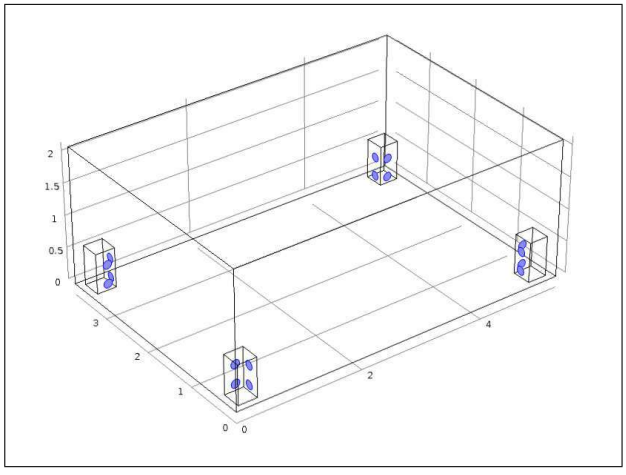

Figure 5. Geometry of the finite element model of the room S with 16 absorbers (in blue) located in the bottom corners.

The results for rooms R1, R2, and R3 are presented in Figures 6a, 6b, and 6c respectively. The modal decay times MT_{60} are displayed as a function of the normalised acoustic resistance θ between 20 Hz and 120 Hz. As expected, these modal decay times increase with the size of the room. As seen in Section 2, for each mode it corresponds an optimal acoustic resistance for the absorber diaphragms for which the modal decay time is minimal. In this configuration, the optimal normalised acoustic resistance should be below 0.1 for the first modes up to 40 Hz.

The ideal frequency-dependent target acoustic resistance to assign to the diaphragms should be optimised, so as to match at best the optimal resistance value of every mode. As illustrated in Figure 6, the absorbers are quite inefficient to make some of the modal decay times shorter, whatever the acoustic resistance value. These modes are thus useless for the optimisation of the target acoustic impedances. From these results, the modes, whose modal decay time varies less than a threshold, are not considered for the optimisation (for normalised acoustic resistances varying between 0.0315 and 1.25). The threshold is arbitrarily chosen a bit shorter than the modal thresholds found in [24], to only keep the modes that are likely to be sufficiently shortened by the absorbers and might be audibly perceptible. With a threshold here equal to

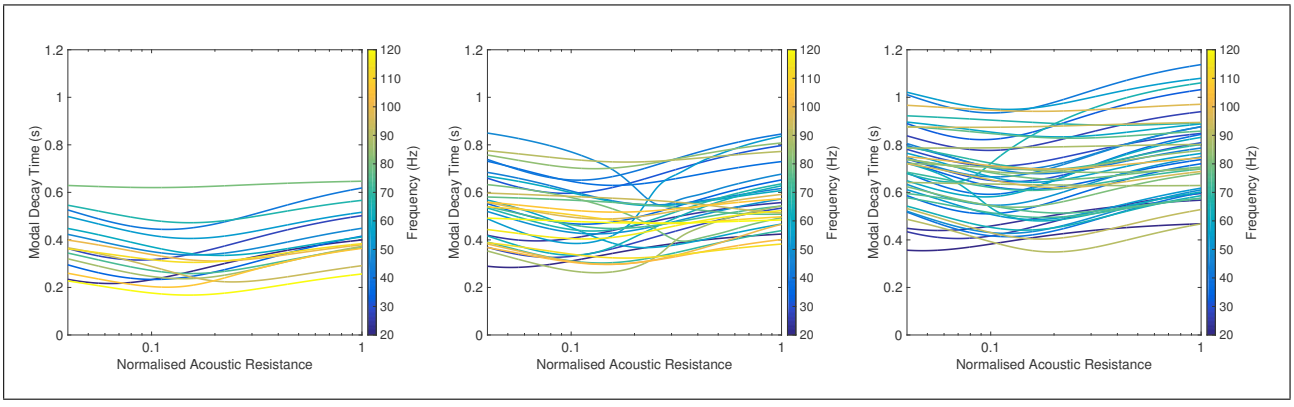

Figure 6. (Colour online) Modal decay times between 20 and 120 Hz depending on the normalised acoustic resistance computed for 16 absorbers located in bottom corners of the rooms (a) R1, (b) R2, and (c) R3.

66 ms, around 75 % of all the modes are kept in the three rooms below 120 Hz. We suggest this threshold should be adapted in function of the dynamics of the modal decay times that are dependent on the wall impedances. Then, for every remaining mode, only the values in an interval equal to $[\min(MT_{60}), \min(MT_{60}) + \tau]$ are kept. The interval should be arbitrarily chosen (here $\tau = 10$ ms) to give a reasonable resistance range around the optimum, mainly for visual representation purposes (how the modal decay times vary depending on the acoustic resistance values at the absorber diaphragms). The results of this selection for the three rooms are summarised in Figure 7, where the modal decay times after selection are projected in the plane (f, θ). Note that few differences can be observed between the three rooms.

Although the optimal acoustic resistance increases with the frequency of the mode, we can hypothesise that the profile of this resistance is the same whatever the room dimensions. This suggests that the target acoustic impedances will be suitable for any room at equivalent wall acoustic impedances.

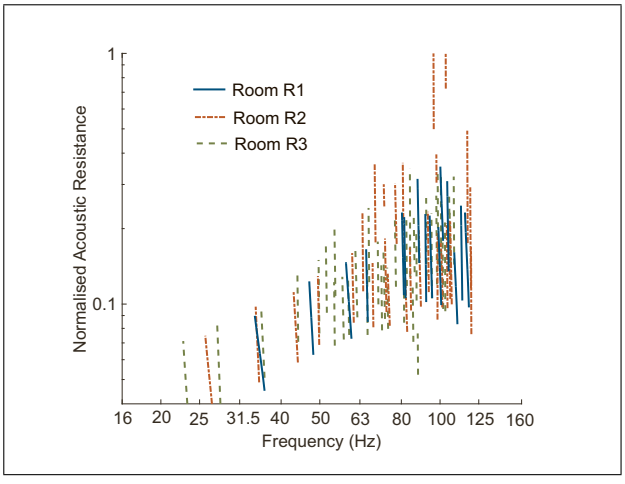

Figure 7. Projection in the plane (f, θ) of modal decay times after selection computed for 16 absorbers located in bottom corners of the rooms R1, R2, and R3.

4. Optimisation of multi-degree-of-freedom target acoustic impedances

From the results found in Section 3, the target acoustic impedances that will be assigned to the electroacoustic absorber diaphragms are now defined, after introducing the acoustic impedance control principle developed in [19]. Then, the target impedances are optimised with the aim of performing the best modal equalisation by minimising the modal decay times in rooms.

4.1. Acoustic impedance control principle

Following a strategy similar to that in [22, 31], the target acoustic impedances should be chosen to approach at best the optimal acoustic resistance values found to minimise all the first modal decay times, by keeping the reactive part very small relative to the resistive part. In [19], a method was presented to achieve a desired specific acoustic impedance at an electroacoustic absorber diaphragm, over a broad frequency range, through an hybrid sensor-/shunt-based impedance control. The mechanical part of the closed-box loudspeaker is modeled as a simple mass - spring - damper system in the low-frequency range, that is the mass M_{ms}, the mechanical compliance C_{mc} accounting for the surround suspension, spider, and acoustic compliance of the enclosure, and the mechanical resistance R_{ms}, respectively. If we denote the effective piston area by S_d and the force factor of the moving-coil transducer by Bl, the equation of motion of the closed-box loudspeaker diaphragm is derived from Newton's second law, which can be written as

$$S_d P_t(\omega) = Z_m V(\omega) + Bl\, I(\omega), \tag{6}$$

where $P_t(\omega)$ is the total sound pressure at the diaphragm, $Z_m(\omega) = \mathrm{j}\omega M_{ms} + R_{ms} + 1/(\mathrm{j}\omega C_{mc})$ is the mechanical impedance of the loudspeaker, $V(\omega)$ is the diaphragm velocity, and $I(\omega)$ is the electrical current flowing through the voice coil. Using only one microphone in front of the diaphragm and taking into account the loudspeaker model in the transfer function implemented in a controller, it is possible to control the diaphragm dynamic response of

the current-driven loudspeaker. Assuming a target specific acoustic impedance $Z_{st}(\omega)$ is realized at the diaphragm, the transfer function from the total sound pressure $P_t(\omega)$ at the diaphragm to the electrical current $I(\omega)$ can be derived from Equation (6) as

$$H(\omega) = \frac{I(\omega)}{P_t(\omega)} = \frac{S_d}{Bl}\left(1 - \frac{Z_m(\omega)}{S_d Z_{st}(\omega)}\right). \tag{7}$$

The specific acoustic impedance at the diaphragm then becomes

$$Z_s(\omega) = \frac{Z_m(\omega)}{S_d - Bl\,H(\omega)}. \tag{8}$$

4.2. Multi-degree-of-freedom target acoustic impedances

If either the mass or the compliance is completely cancelled, the gain of the transfer function $H(\omega)$ in Equation (7), at low or high frequencies respectively, is infinite, which is not technically feasible, because of the limitation of the electrical current delivered by the controller. A general target specific acoustic impedance $Z_{st}(\omega)$ was then introduced in [19], which was expressed with one (or two) reduction factor(s) μ (or μ_M and μ_C) and a target specific acoustic resistance R_{st} as

$$Z_{st}(\omega) = R_{st} + \mathrm{j}\left(\omega\frac{\mu_M M_{ms}}{S_d} - \frac{\mu_C}{\omega S_d C_{mc}}\right). \tag{9}$$

With the formulation of target acoustic impedance in Equation (9), although it is possible to modify the centre frequency f_c of the electroacoustic absorber, only one acoustic resistance value can be assigned to the diaphragm. A MDOF target normalised acoustic impedance is thus defined from n one-degree-of-freedom (one-DOF) impedances in parallel as

$$\zeta_{t_{n-DOF}}(\omega) = \frac{1}{\sum_{k=1}^{n}\frac{1}{\zeta_{t_k}(\omega)}} \tag{10}$$

for $n \geq 2$, where

$$\zeta_{st_k}(\omega) = \theta_{t_k} + \mathrm{j}\left(\frac{\omega M_{ms}}{S_d \nu_{2k-1} Z_c} - \frac{1}{\omega\, S_d \nu_{2k} Z_c C_{mc}}\right) \tag{11}$$

is equivalent to the one-DOF acoustic impedance in Equation (9). The terms ν_{2k-1} and ν_{2k} for $k = [1, n]$ are factors that decrease the effective mass M_{ms}/ν_{2k-1} and effective stiffness $1/(\nu_{2k} C_{mc})$ respectively, so as to extend the sound absorption bandwidth [19]. To keep both the natural mass- and compliance behaviour at low and high frequencies of the MDOF target normalised acoustic impedance equal to those of the one-DOF target normalised acoustic impedance $\zeta_{t_{1-DOF}}(\omega) = \theta_{t_1} + j(\omega M_{ms}/(S_d \nu_{M_1} Z_c) - 1/(\omega\, S_d \nu_{C_1} Z_c C_{mc}))$, where $\nu_{M_1} = \nu_1$ and $\nu_{C_1} = \nu_2$ are fixed values, the conditions are

$$\nu_1 = \nu_{M_1} - \sum_{k=2}^{n}\nu_{2k-1}, \quad \nu_{2n} = \nu_{C_1} - \sum_{k=1}^{n-1}\nu_{2k}. \tag{12}$$

4.3. Figure of merit of electroacoustic absorbers

From the results obtained in Section 2.3 where the absorber is under grazing incidence, the particle velocity is locally almost normal to the electroacoustic absorber diaphragm. Thus, we hypothesise that the sound waves are mainly under normal incidence in front of the absorber diaphragms for the optimisation process. To evaluate the absorption performance of the electroacoustic absorber, we define a figure of merit from the sound absorption coefficient in Equation (2), with respect to the normalised acoustic resistance θ under normal incidence, as

$$\tilde{\alpha}(f, \theta) = 1 - \left|\frac{\zeta(f) - \theta}{\zeta(f) + \theta}\right|^2. \tag{13}$$

This way, the absorption capabilities can be determined in relation to the frequency for any normalised acoustic resistance.

In addition, a bandwidth BW of efficient sound absorption was defined in [19], as the frequency range over which the total sound intensity in front of the diaphragm is less than twice the total sound intensity in the ideal case ($\alpha = 1$). This criterion corresponds to a threshold value of minimal efficient sound absorption: $\alpha_{th} = 1-(\sqrt{2}-1)^2 \simeq 0.83$. As this criterion is relevant in a duct, this threshold value is also applied for the figure of merit of electroacoustic absorbers for the room modal equalisation.

4.4. Weighting function of optimal acoustic resistances

To take into account the results found in Section 3 for the optimisation of the MDOF target acoustic impedance expressed in Equation (10), a profile $\theta_p(f)$ is estimated from a polynomial of second order to fit at best all the normalised acoustic resistances corresponding to the minimal modal decay times illustrated in Figure 7, between 16 Hz and 100 Hz. Above 100 Hz, the profile $\theta_p(f)$ is chosen constant and equal to the normalised acoustic resistance value at 100 Hz. Although the simulations were calculated for only three rooms in Section 3, the optimal acoustic resistances should follow this profile for any room. The discrete optimal acoustic resistances illustrated in Figure 6 are then turned into a weighting function, which is defined through a Gaussian-based function as

$$W_{opt}(f, \theta) = \left(a_1 f + b_1\right)\exp\left[-\frac{\left(\theta - g\,\theta_p(f)\right)^2}{2\left(a_2 f + b_2\right)}\right], \tag{14}$$

where a_1 and a_2 are coefficients of the frequency f and b_1 and b_2 are the constant terms of two linear functions respectively, and g is an overall coefficient of the profile $\theta_p(f)$. This way, the maximal magnitude and standard deviation of the Gaussian-based function vary according to both linear functions. The parameter values are chosen to give more importance to the first modes between 20 Hz and 40 Hz, and give less importance to the modes higher than 80 Hz. The coefficient g is also chosen below 1, so that the figure of merit, expressed in Equation (13), covers

Table II. Parameters used for the weighting function of optimal acoustic resistances.

a_1	b_1	a_2	b_2	g
$-5 \cdot 10^{-5}$	0.013	$-25 \cdot 10^{-5}$	0.065	0.75

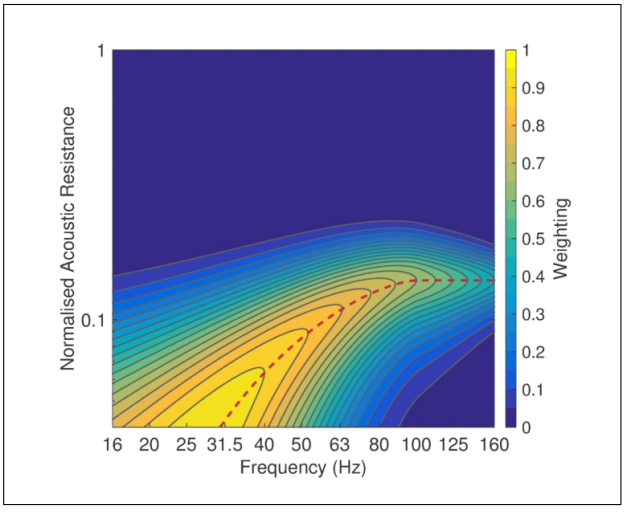

Figure 8. (Colour online) Frequency – normalised acoustic resistance map of the weighting function for the optimisation of the target normalised acoustic resistance. The red dotted line depicts the profile $\theta_p(f)$ multiplied by the coefficient g.

at best the minimal values of the optimal acoustic resistance of all the modes depicted in Figure 7. The parameter values of the weighting function $W_{opt}(\theta, f)$ are summarised in Table II.

Figure 8 illustrates the frequency – normalised acoustic resistance map of the weighting function of optimal normalised acoustic resistances. The red dotted line depicts the profile $\theta_p(f)$ multiplied by the coefficient g.

4.5. Optimisation strategy

To maximise the performance of the electroacoustic absorbers for the room modal equalisation, the normalised acoustic resistances at the diaphragms should be as close as possible of the profile $\theta_p(f)$. As it is not possible to assign purely resistive impedances at the loudspeaker diaphragms (see Section 4.2), the acoustic reactance should be taken into account in the optimisation process through the figure of merit defined in Section 4.4, so as to evaluate the global effect of the impedance on the performance of absorbers to damp the modes. A parametric optimisation is proposed through an objective method using the simplex search method developed in [32]. The objective function is defined according to the figure of merit $\tilde{\alpha}(f, \theta)$ and weighting function $W_{opt}(f, \theta)$ expressed in Equations (13) and (14) respectively, as

$$\mathcal{A}_2 = \int\int \max\left(\tilde{\alpha}(f,\theta) - \alpha_{th}, 0\right) W_{opt}(f,\theta)\,\mathrm{d}f\,\mathrm{d}\theta. \qquad (15)$$

By maximising this objective function, expressed in Hz, the figure of merit is maximised depending on the weighting function, over frequency and normalised acoustic resistance ranges as large as possible, that is $\tilde{\alpha}(f, \theta) \geq \alpha_{th}$, so as to approach at best the optimal acoustic resistance values of the first room modes. The optimisation is limited to finding the factors ν_{2k-1} and ν_{2k} and target normalised acoustic resistances θ_{t_k} for $k = [1, n]$, depending on the fixed values of factors ν_{M_1} and ν_{C_1} expressed in Equations (12) and (12) respectively.

4.6. Performance analysis

The performance of the electroacoustic absorbers for the room modal equalisation is estimated considering the Peerless SDS-P830657 loudspeaker mounted in a closed-box of volume $V_b = 10\,\mathrm{dm}^3$. The equivalent mechanical compliance is $C_{mc} = 242.35\ \mu\mathrm{m{\cdot}N^{-1}}$ and the moving mass is $M_{ms} = 14.67\,\mathrm{g}$. A diminution of 84 % of the effective mass of the loudspeaker is imposed, that is $\nu_{M_1} = 6.25$, so as to improve the absorption performance [19], and thus minimise as many modal decay times as possible. Also, the centre frequency f_c, which is equal to 84.4 Hz when the electroacoustic absorber is in open circuit, should be lowered through the factor ν_{C_1}, so as to get closer to the first eigenfrequencies. If we want to ensure a proper functioning of the electroacoustic absorbers up to a certain sound pressure level in a given room, the maximal value of electrical current delivered by the controller is limited by technical specifications. As the magnitude of the transfer function $H(\omega)$ in Equation (7) is directly dependent on the factors ν_{M_1} and ν_{C_1}, the factor ν_{C_1} is chosen equal to 25.00, which results in dividing the centre frequency f_c by two.

Table III summarizes the parameters for the different cases under study. The case C0 corresponds to the basic configuration of the electroacoustic absorber in open circuit. Cases C1, C2, and C3 correspond to the one-DOF, two-DOF, and three-DOF target normalised acoustic impedances respectively.

Figure 9 illustrates the real and imaginary parts of the normalised acoustic impedance at the electroacoustic absorber diaphragm computed in cases C1, C2, and C3, relative to the basic configuration (case C0). The red dotted line depicts the profile $\theta_p(f)$. Thanks to the one-DOF impedances in parallel, the imaginary part of the target normalised acoustic impedances in cases C2 and C3 is closer to zero over a wider frequency band than that in case C1. The target normalised acoustic resistance is constant in case C1 and is equal to 0.126, it varies between 0.075 and 0.200 in case C2, and between 0.052 and 0.202 in case C3. The higher the number of degrees of freedom of the target normalised acoustic impedance, the larger the variations of the normalised acoustic resistance, and the greater the deviation from the profile $\theta_p(f)$ for the modes at higher frequencies.

To compare the performance for the room modal equalisation between the four cases, the figure of merit $\tilde{\alpha}(\theta, f)$ defined in Equation (13) is computed in every case. The set of points of the plane (f, θ) such as $\tilde{\alpha}(f, \theta) = \alpha_{th}$ is displayed in every case in Figure 10, as well as the

Table III. Parameter values of the optimised one-, two-, and three-DOF target normalised acoustic impedances (cases C1, C2, and C3) relative to the basic configuration of the open circuit electroacoustic absorber (case C0).

Case	ζ_{t_1}			ζ_{t_2}			ζ_{t_3}			f_c (Hz)
	θ_{t_1}	ν_1	ν_2	θ_{t_2}	ν_3	ν_4	θ_{t_3}	ν_5	ν_6	
C0	0.210	1.00	1.00	-	-	-	-	-	-	84.4
C1	0.126	6.25	25.00	-	-	-	-	-	-	42.2
C2	0.162	2.16	2.36	0.134	4.09	22.64	-	-	-	42.2
C3	0.208	1.86	2.86	0.133	1.32	1.11	0.139	3.07	21.03	42.2

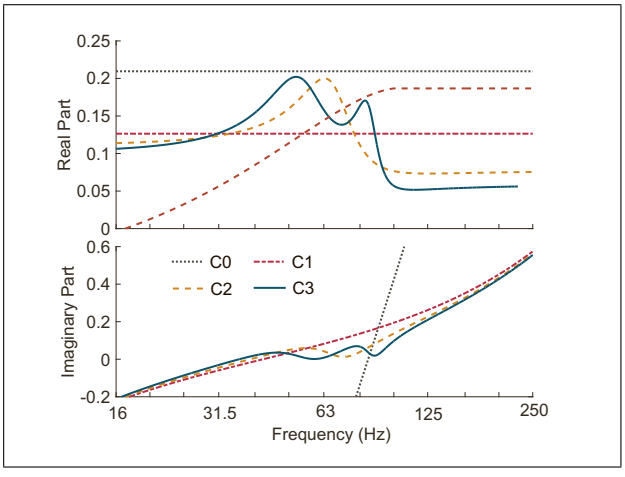

Figure 9. Real and imaginary parts of the target normalised acoustic impedance at the electroacoustic absorber diaphragm, computed for the one-, two- and, three-DOF target impedances optimised from the objective function of area over threshold, relative to the basic configuration. The red dotted line depicts the profile $\theta_p(f)$.

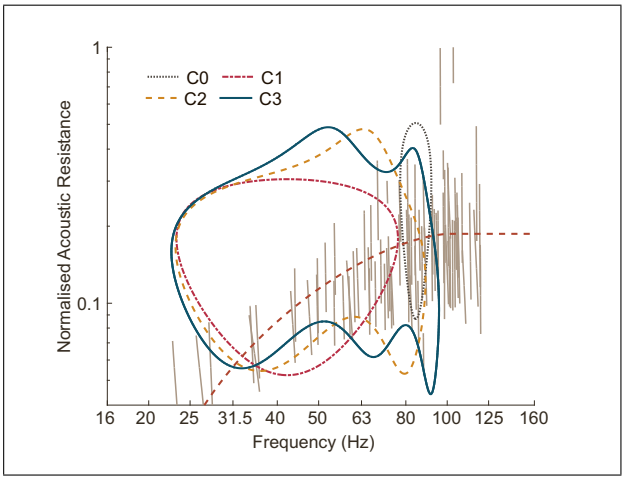

Figure 10. Set of points of the plane (f, θ) such as $\tilde{\alpha}(f, \theta) = \alpha_{th}$ computed in cases C0, C1, C2, and C3. The beige solid lines depict the projection in the plane (f, θ) of modal decay times after selection computed for 16 absorbers located in bottom corners of the rooms R1, R2, and R3. The red dotted line depicts the profile $\theta_p(f)$.

modal decay times after selection illustrated in Figure 7 (in beige solid lines). The red dotted line depicts the profile $\theta_p(f)$. Thanks to the chosen values for the terms ν_1 and ν_{M_1} making the center frequency f_c decrease, the areas defined by this set of points in cases C1, C2, and C3 are larger than that in case C0. Although these areas include the optimal normalised acoustic resistances for the first modes in the three cases, the upper bound along the frequency axis is higher in case C2 than that in case C1, and even more in case C3. The best possible performance of the electroacoustic absorbers for room modal equalisation is thus expected in case C3, where a significant effect on modal decay times is expected at frequencies as low as 25 Hz. Note that the areas include the majority of the minimal values of the optimal normalised acoustic resistances of the first modes, thanks to the coefficient g expressed in Equation (14).

5. Experimental results

5.1. Experimental setup

To validate the results found in Section 4, the performance of the electroacoustic absorber was experimentally evaluated in each case by measuring the frequency response of the normalised acoustic impedance at the diaphragm in a waveguide of length $L = 1.97$ m and internal diameter $\varnothing = 150$ mm, according to the ISO 10534-2 standard [33]. The measurement procedure was the same as the one described in [19]. The duct was closed by electrodynamic loudspeakers in closed boxes of volume $V_b = 10\,\mathrm{dm}^3$. The sound source delivered a band-limited pink noise of bandwidth [2 Hz - 2 kHz]. Three 1/2" PCB 378B02 microphones were wall-mounted at positions $x_1 = 1.02$ m, $x_2 = 1.51$ m, and $x_3 = 1.62$ m from the sound source, measuring the sound pressures $p_1 = p(x_1, t)$, $p_2 = p(x_2, t)$, and $p_3 = p(x_3, t)$. The frequency responses $H_{13} = p_3/p_1$ and $H_{23} = p_3/p_2$ were processed through a Brüel and Kjær Pulse multichannel analyser (type 3160). With this setup, the electroacoustic absorber performance is evaluated for plane waves under normal incidence over a frequency range 44–1340 Hz. To focus the evaluation on the frequency range of interest, the results are displayed up to 500 Hz.

To asssign the different MDOF target acoustic impedances at the diaphragm of an electroacoustic absorber, we used the hybrid sensor-/shunt-based impedance control with the same electroacoustic absorber as the one used in [19], whose loudspeaker model parameters are presented in Section 4.2. Only the electronic part of the

impedance control was different. The sound pressure in front of the diaphragm used as input signal for the control was measured thanks to a 1/4" electret microphone with its preamplification circuit. The transfer function $H(\omega)$ in Equation (7) was implemented onto an Analog Devices digital signal processor (Sharc processor), with a measured time delay equal to 18.1 μs. The signals were converted thanks to Analog Devices analog-to-digital and digital-to-analog converters. The voltage controlled current source was an operational amplifier-based improved Howland current pump circuit [34].

5.2. Acoustic impedance measurement

Cases C0, C1, C2 and C3, whose parameters are summarised in Table III, were used for the measurements. The measured frequency response of the normalised acoustic impedance in every case is presented in Figure 11. Thanks to the control, both the acoustic resistance and reactance at the diaphragm are modified to reach as close as possible the target acoustic impedances. In cases C1, C2 and C3, even though a slight shift in frequency is visible, the magnitude is kept below one fifth, and the phase is closer to zero over a broader frequency range than in case C0 (when the control is switched off). The slight differences can be attributed to imperfections in the lumped element model and to the frequency response of the microphone, which was not taken into account in the control law.

The figure of merit $\tilde{\alpha}(\theta, f)$ expressed in Equation (13) is computed from the measured frequency responses of the normalised acoustic impedance in every case. The set of points of the plane (f, θ) such as $\tilde{\alpha}(f, \theta) = \alpha_{th}$ is displayed in every case in Figure 12, as well as the modal decay times after selection illustrated in Figure 7 (in beige solid lines).

The red dotted line depicts the profile $\theta_p(f)$. The measurements are satisfactorily consistent with the corresponding computations illustrated in Figure 10. With three degrees of freedom (case C3), the large area defined by the set of points of the plane (f, θ) covers the whole values of optimal acoustic resistances found in Section 3, except for the first three modes. Nevertheless, with a higher value of factor v_{C_1}, and if the technical specifications make it possible, the first modes could be covered by this area as well. Thus we may expect good performance of electroacoustic absorbers for the equalisation of the first modes in actual small rooms.

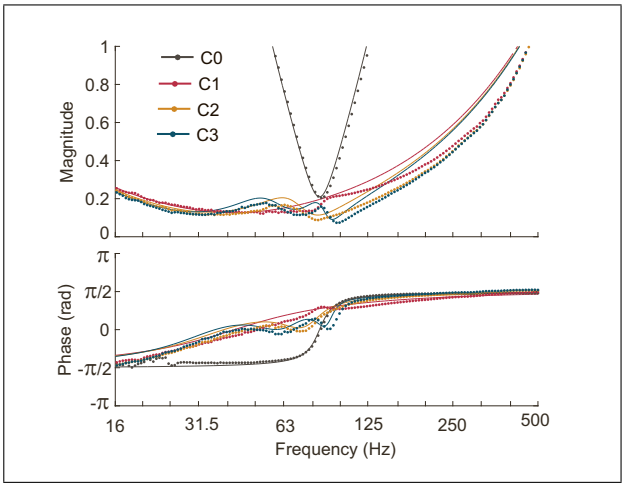

Figure 11. Frequency responses of the normalised acoustic impedance at the electroacoustic absorber diaphragm computed (solid lines) and measured (dotted lines) in cases C0, C1, C2, and C3.

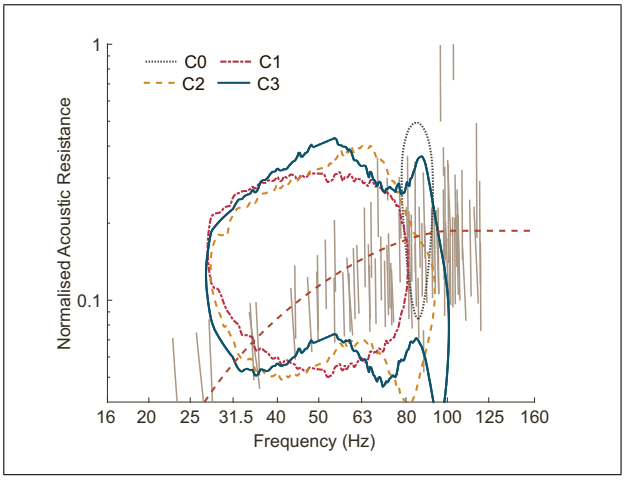

Figure 12. Set of points of the plane (f, θ) such as $\tilde{\alpha}(f, \theta) = \alpha_{th}$ computed in cases C0, C1, C2, and C3 from the corresponding measured acoustic impedances. The beige solid lines depict the projection in the plane (f, θ) of modal decay times after selection computed for 16 absorbers located in bottom corners of the rooms R1, R2, and R3. The red dotted line depicts the profile $\theta_p(f)$.

6. Conclusion

In this paper, the effect of electroacoustic absorbers on the minimisation of the modal decay times was investigated. For the simulation, the absorbers were modelled by flat disks, where a purely resistive acoustic impedance was assigned to each absorber. Two numerical studies in a duct showed that the absorber causes a significant decrease of the modal decay times, whether its diaphragm is oriented normal to the propagation dimension (normal incidence) or parallel to it (grazing incidence). For every mode, the optimal acoustic resistance is dependent on the mode and absorber area: the larger the area, the lower the modal decay times.

The effect of the room dimensions has also been studied from the simulation of three rectangular rooms of different dimensions. A given layout of a possible actual implementation of electroacoustic absorbers, with a fixed total area, was proposed. It was shown that the optimal acoustic resistances for which a minimal modal decay time is obtained, has the same frequency-dependent profile, whatever the room dimensions for a given wall impedance value. As the reactive part of the acoustic impedances at the absorber diaphragms is dominant at very low and high frequencies,

further work should include the effect of the acoustic reactances at the diaphragms in the modelling.

Then, taking into account the results of the simulations with the given layout of absorbers in the bottom corners of the studied rooms, multi-degree-of-freedom target acoustic impedances at the diaphragms were optimised to maximise the performance for the modal equalisation. The acoustic impedances approach at best the optimal resistance value found to minimise each modal decay time, by keeping the reactive part very small relative to the resistive part.

Finally, the performance of the electroacoustic absorber was experimentally evaluated in a waveguide, by measuring the acoustic impedance for each optimised MDOF target acoustic impedance. The best performance is obtained for the three-DOF acoustic impedance, providing the best fit to the optimal profile of acoustic resistances. Although higher DOF target acoustic impedances could also be achieved, the performance might be limited by technological specifications, such as the maximal value of electrical current delivered by the controller.

The performance of the electroacoustic absorbers for the modal equalisation was also evaluated in actual listening rooms, whose results can be found in [35], confirming the efficiency of the concept to shorten the modal decay times. The method presented in this paper could also be used for other applications requiring specific values of acoustic impedance over a given frequency range.

Acknowledgements

The authors would like to thank Torje Nikolai Thorsen and Quentin Berthet for the development of the electronic part for the experimental measurements.

References

[1] H. Kuttruff: Acoustics: an introduction. CRC Press, 2007.

[2] J. Voetmann, J. Klinkby: Review of the low-frequency absorber and its application to small room acoustics. Audio Engineering Society Convention 94, 1993, Audio Engineering Society.

[3] O. J. Bonello: A new criterion for the distribution of normal room modes. Journal of the Audio Engineering Society **29** (1981) 597–606.

[4] R. Walker: Optimum dimension ratios for small rooms. Audio Engineering Society Convention 100, 1996, Audio Engineering Society.

[5] T. J. Cox, P. D'Antonio, M. R. Avis: Room sizing and optimization at low frequencies. Journal of the Audio Engineering Society **52** (2004) 640–651.

[6] K. O. Ballagh: Optimum loudspeaker placement near reflecting planes. Journal of the Audio Engineering Society **31** (1983) 931–935.

[7] X. Shen, Y. Shen, J. Zhou: Optimization of the locations of the loudspeaker and absorption material in a small room. Applied acoustics **65** (2004) 791–806.

[8] T. Welti, A. Devantier: Low-frequency optimization using multiple subwoofers. Journal of the Audio Engineering Society **54** (2006) 347–364.

[9] N. Stefanakis, J. Sarris, G. Cambourakis: Source placement for equalization in small enclosures. Journal of the Audio Engineering Society **56** (2008) 357–371.

[10] M. Miyoshi, Y. Kaneda: Inverse filtering of room acoustics. IEEE Transactions on Acoustics, Speech, and Signal Processing **36** (1988) 145–152.

[11] S. J. Elliott, P. A. Nelson: Multiple-point equalization in a room using adaptive digital filters. Journal of the Audio Engineering Society **37** (1989) 899–907.

[12] S. J. Elliott, L. P. Bhatia, F. S. Deghan, A. H. Fu, M. S. Stewart, D. W. Wilson: Practical implementation of low-frequency equalization using adaptive digital filters. Journal of the Audio Engineering Society **42** (1994) 988–998.

[13] F. Asano, D. Swanson: Sound equalization in enclosures using modal reconstruction. The Journal of the Acoustical Society of America **98** (1995) 2062–2069.

[14] S. J. Elliott, P. Joseph, P. A. Nelson, M. E. Johnson: Power output minimization and power absorption in the active control of sound. The Journal of the Acoustical Society of America **90** (1991).

[15] A. Mäkivirta, P. Antsalo, M. Karjalainen, V. Välimäki: Modal equalization of loudspeaker-room responses at low frequencies. Journal of the Audio Engineering Society **51** (2003) 324–343.

[16] A. O. Santillán, C. S. Pedersen, M. Lydolf: Experimental implementation of a low-frequency global sound equalization method based on free field propagation. Applied Acoustics **68** (2007) 1063–1085.

[17] C. S. Pedersen, H. Møller: Sound field control for a low-frequency test facility. Audio Engineering Society Conference: 52nd International Conference: Sound Field Control-Engineering and Perception, 2013, Audio Engineering Society.

[18] A. Celestinos, S. B. Nielsen: Controlled acoustic bass system (cabs) a method to achieve uniform sound field distribution at low frequencies in rectangular rooms. Journal of the Audio Engineering Society **56** (2008) 915–931.

[19] E. Rivet, S. Karkar, H. Lissek: Broadband low-frequency electroacoustic absorbers through hybrid sensor- /shunt-based impedance control. IEEE Transactions on Control Systems Technology **25** (2017) 63–72.

[20] R. Boulandet, E. Rivet, H. Lissek: Sensorless electroacoustic absorbers through synthesized impedance control for damping low-frequency modes in cavities. Acta Acustica united with Acustica **102** (2016) pp. 696–704(9).

[21] V. Martin, A. Bodrero: An introduction to the control of sound fields by optimising impedance locations on the wall of an acoustic cavity. Journal of Sound and Vibration **204** (1997) 331–357.

[22] N. Sellen, M. Cuesta, M.-A. Galland: Noise reduction in a flow duct: Implementation of a hybrid passive/active solution. Journal of Sound and Vibration **297** (2006) 492–511.

[23] B. Betgen, M.-A. Galland, E. Piot, F. Simon: Implementation and non-intrusive characterization of a hybrid active–passive liner with grazing flow. Applied Acoustics **73** (2012) 624–638.

[24] B. M. Fazenda, M. Stephenson, A. Goldberg: Perceptual thresholds for the effects of room modes as a function of modal decay. The Journal of the Acoustical Society of America **137** (2015) 1088–1098.

[25] J. H. Rindel: A note on modal reverberation times in rectangular rooms. Acta Acustica united with Acustica **102** (2016) 600–603.

[26] P.-J. René: Contributions aux études sur le couplage électroacoustique dans les espaces clos en vue du contrôle actif. Dissertation. Ecole Polytechnique Fédérale de Lausanne (EPFL), 2006.

[27] M. Meissner: Influence of wall absorption on low-frequency dependence of reverberation time in room of irregular shape. Applied Acoustics **69** (2008) 583–590.

[28] V. Pagneux, N. Amir, J. Kergomard: A study of wave propagation in varying cross-section waveguides by modal decomposition. part i. theory and validation. The Journal of the Acoustical Society of America **100** (1996) 2034–2048.

[29] L. M. Campos, J. M. Oliveira: On sound generation in cylindrical flow ducts with non-uniform wall impedance. International Journal of Aeroacoustics **12** (2013) 309–347.

[30] L. Cremer: Theorie der Luftschalldämpfung mit schluckender Wand und das sich dabei ergebende höchste Dämpfungsmaß. Acustica, Akust. Beihefte **3** (1953) 249–263.

[31] J.-B. Dupont, M.-A. Galland: Active absorption to reduce the noise transmitted out of an enclosure. Applied Acoustics **70** (2009) 142–152.

[32] J. C. Lagarias, J. A. Reeds, M. H. Wright, P. E. Wright: Convergence properties of the Nelder–Mead simplex method in low dimensions. SIAM Journal on optimization **9** (1998) 112–147.

[33] I. 10534-2-1998: Acoustics - determination of sound absorption coefficient and impedance in impedance tubes - part 2 : Transfer-function method. Tech. Rept. Internation Standard Organization, Geneva, Switzerland, 1998.

[34] R. A. Pease: A comprehensive study of the howland current pump. National Semiconductor **29** (January 2008) 1–17.

[35] E. Rivet, S. Karkar, H. Lissek, T. N. Thorsen, V. Adam: Experimental assessment of low-frequency electroacoustic absorbers for modal equalization in actual listening rooms. Audio Engineering Society Convention 140, May 2016.